Journal of
Instrumentation

Automated characterisation and operational insights of superconducting travelling wave parametric amplifiers: unveiling novel behaviours and enhancing tunability

Published by IOP Publishing for Sissa Medialab

Received: *January 22, 2024*
Accepted: *June 14, 2024*
Published: *August 28, 2024*

Automated characterisation and operational insights of superconducting travelling wave parametric amplifiers: unveiling novel behaviours and enhancing tunability

S. Wood[a,*] **N. Klimovich**[b] **and B.-K. Tan**[b]

[a]*The Queen's College, University of Oxford, High Street, Oxford OX1 4AW, United Kingdom*
[b]*Department of Physics (Astrophysics), University of Oxford, Denys Wilkinson Building, Keble Road, Oxford OX1 3RH, United Kingdom*

E-mail: samuel.wood@queens.ox.ac.uk

Abstract: Superconducting travelling wave parametric amplifiers (TWPAs) exhibit great promise across various applications, owing to their broadband nature, quantum-limited noise performance, and high-gain operation. Whilst their construction is relatively simple, particularly for thin-film-based TWPAs, challenges such as the requirement for an extremely long transmission line, current fabrication limitations, and their sensitivity to fabrication tolerances, mean that their optimal operating conditions often differ from those anticipated during the design stage. As a result, manual fine-tuning of numerous operational parameters becomes necessary to recover optimal performance; a process that is both labour-intensive and time-consuming. This paper introduces an automated methodology designed to significantly accelerate the characterisation of a TWPA by several orders of magnitude without requiring human intervention. Additionally, we have developed metrics to condense the multitude of measured frequency responses of the TWPA, obtained in data cube form, into an easily-understandable format for further scientific interpretation. To demonstrate the efficacy and speed of our methodology, we utilise an existing NbTiN (niobium titanium nitride) TWPA as an example. This showcases the capability of our approach to unveil both broad- and fine-scale behaviours of the device, highlighting the importance of an automated experimental setup for the in-depth investigation of TWPAs for future developments.

Keywords: Data acquisition concepts; Data reduction methods; Instrument optimisation; Superconductive detection materials

*Corresponding author.

https://doi.org/10.1088/1748-0221/19/08/P08024

Contents

1 Introduction

The last decade has seen a rise in the research and development of superconducting parametric amplifiers (SPAs), especially the travelling wave parametric amplifier (TWPA) technology. This is in part spurred by the need for low-noise amplification at microwave frequencies by many applications; for instance within the quantum computing and radio astronomy [1–3] communities. TWPAs can provide high gain over broad bandwidth, with quantum-limited noise [4, 5]. To achieve amplification, the device is injected with an AC 'pump' tone, and in some cases a DC bias current as well, in conjunction with the 'signal' tone intended for amplification. The nonlinear medium of the TWPA facilitates a wave-mixing process, enabling interaction between the weak signal tone, and the strong pump tone and DC bias current. The result is the transfer of energy from the pump/DC to the signal, thereby accomplishing amplification. This yields three interacting parameters that can be altered to control the gain-bandwidth performance of the TWPA: pump frequency, pump power, and DC bias current.[1]

While the exact values of these parameters are typically well-established through meticulous theoretical simulations [6–10], the reality of fabrication introduces potential inaccuracies. Factors like the uniformity of surface impedance in the superconducting film and fabrication defects can make the true optimal operating conditions uncertain. The incorporation of dispersion control elements,

[1]A more sophisticated operation mode, involving two pump tones without DC biasing, would yield four interdependent parameters.

2024 JINST 19 P08024

necessary for achieving high gain via phase-matching condition and suppressing unwanted modes, further complicates both the fabrication and operation. Additionally, existing theoretical models used for predicting TWPA operation, mainly the coupled mode equation models [1, 11, 12], often focus on only a few fundamental frequency modes. Neglecting higher harmonics in practice may impact the TWPA's performance [13].

Moreover, it is noteworthy that TWPAs exhibit versatility; they can be retuned to operate in different wave-mixing regimes, such as three-wave mixing or four-wave mixing [14–20], or even serve different functionalities altogether, such as acting as a frequency converter [21]. The interplay among pump frequency, pump power, and DC bias is challenging to vary independently, as the device behaviour is very sensitive to their exact values, making the path to seek an optimised operating configuration non-trivial. This in turn implies that exploring the extensive operational parameter spaces through manual fine-tuning of the complicated setups required to measure the performance of these TWPAs is time-consuming and exhaustive. In this paper, we introduce a methodology that leverages software and hardware automation to enable efficient and detailed characterisation of TWPAs. We then demonstrate its efficacy by applying our methodology to a NbTiN (niobium titanium nitride) TWPA designed to operate in the three-wave mixing regime.

2 Experimental setup

2.1 Operation of TWPAs

The TWPA under test used to demonstrate our methodology presented in this paper is developed based on high kinetic inductance film (termed a kinetic inductance TWPA), exploiting the nonlinear kinetic inductance of thin superconducting transmission lines[2] to enable wave mixing and promote high gain [1]. TWPAs can operate in either a four-wave mixing (4WM) or three-wave mixing (3WM) mode. The former requires an AC pump tone ω_p to be mixed with the signal ω_s to produce amplification bands centred around the pump frequency, while the latter requires both the AC pump tone and a DC bias I_DC, producing an amplification band centred at half the pump frequency. An extensive overview of the theory of their operation is provided in other literature and largely depends on the engineered dispersion of the superconducting transmission line [6, 13, 16, 23].

As an illustrative example, when the dispersion allows for optimal phase matching between the pump and signal tones in a 3WM process, the gain of the TWPA is exponential:

$$G_\mathrm{3WM} = \frac{1}{4}\exp\left(\frac{k_\mathrm{p}\left|I_\mathrm{p}\right|\left|I_\mathrm{DC}\right|L}{4I_*^2}\right) \tag{2.1}$$

where L is the transmission line length, k_p is the wavenumber of the pump, I_p is the amplitude of the pump current, and I_* is a constant that sets the scale of the nonlinearity of the kinetic inductance. However, in cases where the dispersion diverges from the optimal phase-matching criterion, the gain profile follows a much more complicated behaviour depending on the operating conditions. As shown in figure 1, a small deviation from nominal parameters in fabrication can result in vastly

[2]Other TWPA variants include Josephson junction and SQUID (superconducting quantum interference device) TWPAs, but their operation is largely similar to KI-TWPAs. Our theory and methodology can be applied to these variants as well, or extended to other SPAs such as the narrower band Josephson Parametric Amplifiers (JPAs) [22].

2024 JINST 19 P08024

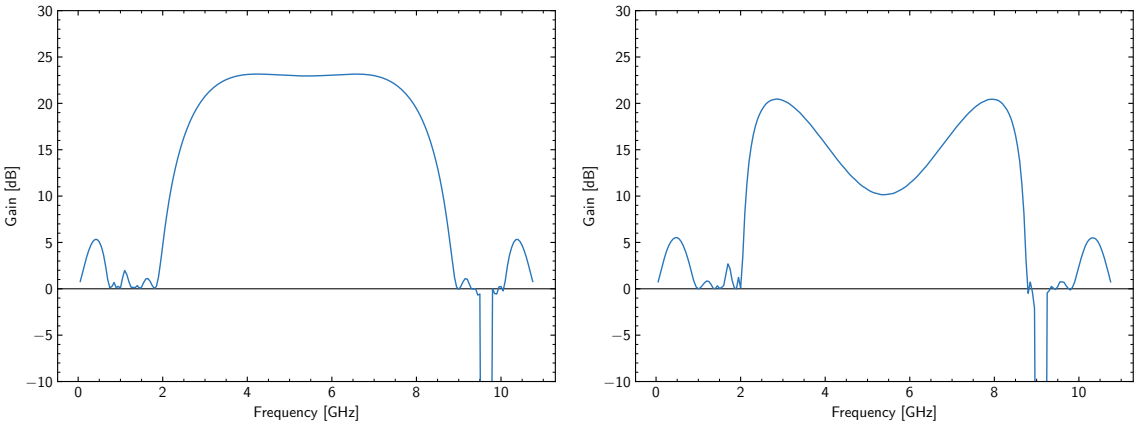

Figure 1. Two exemplary theoretical gain curves, demonstrating how a slight variation in the TWPA's intrinsic parameters (e.g. due to fabrication limitations) can result in vastly different performance for the same design. The left panel shows the designed performance, while the right panel shows the same operating conditions with the superconducting film surface resistivity being 5 % higher than intended, caused by fabrication tolerances.

different performance, requiring experimental tuning of operating conditions to recover the desired flat and broadband gain.

2.2 Device-under-test and measurement setup

The device-under-test (DUT) used to demonstrate our concept is a kinetic-inductance-based TWPA comprising a long NbTiN microstrip transmission line designed to operate in the 3WM regime. The details of the KI-TWPA design can be found in [24, 25]. Note that this device is chosen as an example simply due to its availability to us to perform the experimental tests, but the methodology described here is applicable to a wide range of SPAs.

Figure 2 shows a typical cryogenic measurement setup used to characterise a TWPA. It allows a pump tone and a weak signal tone (provided by a signal generator and a vector network analyser (VNA) respectively) to be combined through a directional coupler and a series of appropriate attenuation stages, to propagate through the TWPA, and return to the second port of the VNA where the gain is measured. The TWPA is kept at ~ 20 mK, and a cryogenic switch allows its operation to be compared with a reference wire, to accurately measure the actual gain of the DUT. The pump (provided by a Hittite HMC-T2100 signal generator in our case) and DC bias (a Keithley 6221 current source, with filtering) are at room temperature. An Anritsu MS4644B VNA measures the small-signal power gain using the S_{21} scattering parameter.

Whilst a gain curve for the TWPA can be obtained by normalising the system's frequency response against the superconducting reference wire, conventionally the gain is presented by normalising the measured profile against the TWPA's response without an AC pump present, to remove systematic effects. Hence, all gain curves that follow in this paper are produced by taking the S_{21} data for a specific configuration of pump frequency, pump power, and DC bias, and normalising that against the S_{21} data without the pump. This is illustrated in figure 3, which shows the change in ripple structure with the applied DC current as well as the gain once the pump is applied.

2024 JINST 19 P08024

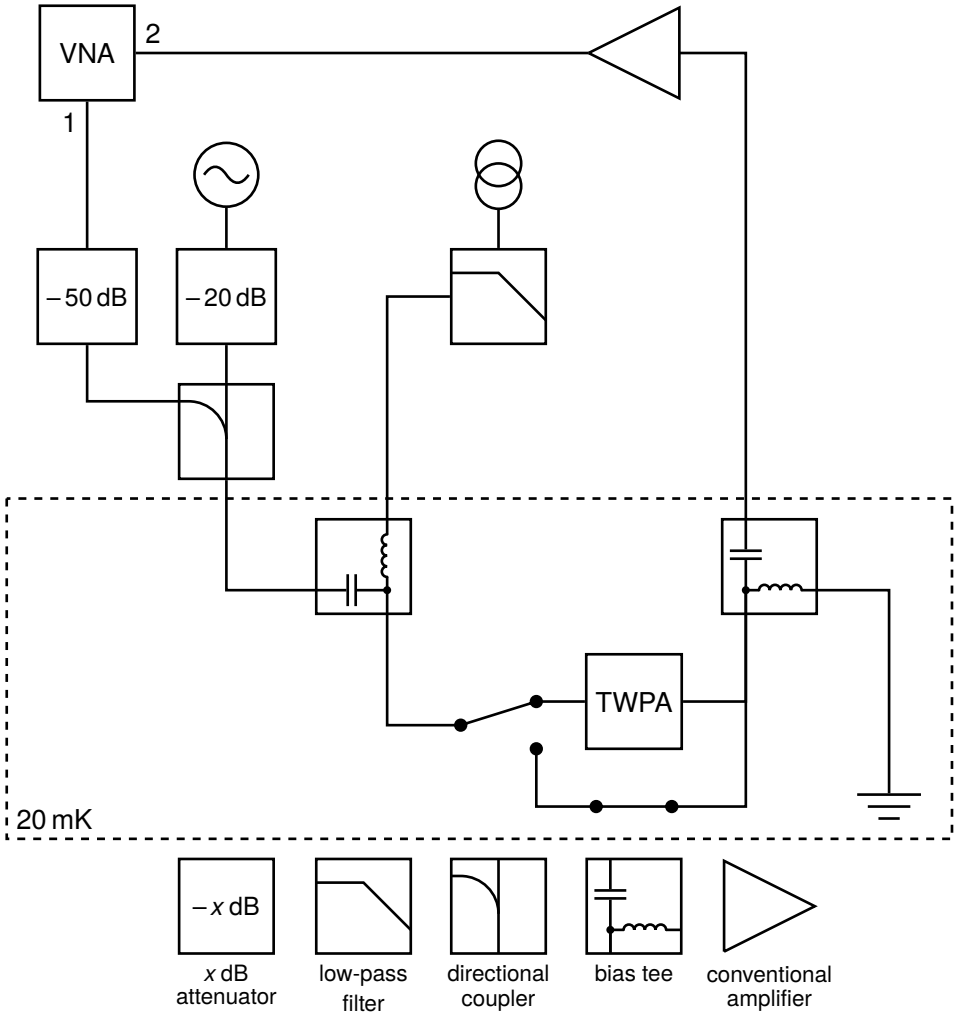

Figure 2. Schematic of measurement setup. The TWPA and reference line are at the 20 mK stage, with the associated measurement equipment at room-temperature.

3 Methodology

3.1 Manually characterising a DUT

A typical procedure required for manually characterising the performance of a (3WM) TWPA is:

1. Sweep with weak signal tones from the VNA to measure the S_{21} profile of the DUT. Find the critical current (I_c) of the device by slowly increasing I_{DC} (without I_p) until the superconducting device returns to its normal state.

2. Set I_{DC} to a chosen value e.g., $I_{DC} = I_c/2$.

3. Pick a pump frequency and increase I_p until the device goes normal ($I_{p,max}$). Reset both I_{DC} and I_p, then set I_{DC} back to the value chosen in step two, and I_p to ~ 3 dB lower than $I_{p,max}$.[3]

[3]If the pump is set too close to the maximum allowable I_p, then as the pump frequency ω_p is swept, small variations in the transmission profile of the DUT will cause the overall current $I_p + I_{DC}$ to exceed the critical current I_c.

2024 JINST 19 P08024

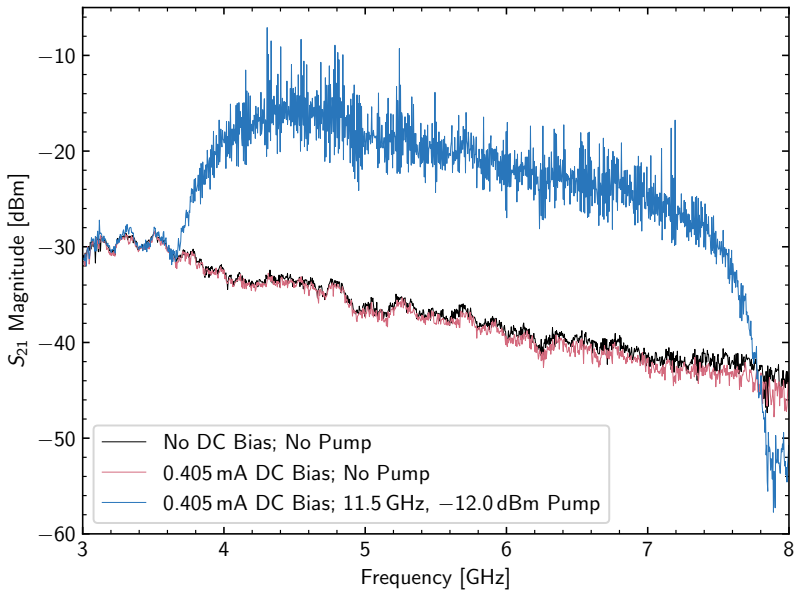

Figure 3. The un-biased and un-pumped S_{21}, biased S_{21}, and transmission measurement with both the pump and bias turned on.

4. Slowly increase ω_p until a noteworthy gain profile is observed.

5. Fix ω_p. Gradually increase I_p until the critical current is reached, to search for maximum gain. Reset the applied currents, adjust I_p back to the optimal point, and record the data.

6. Repeat steps three to five until all the potential parameter spaces of ω_p and I_p have been exhausted.

7. Go back to step two and choose another value for I_{DC}. Repeat steps three to six, until an optimal gain-bandwidth profile is obtained.

It is apparent that a thorough manual search for an optimal gain-bandwidth product would be both tedious and time consuming. The three experimentally-controlled parameters of I_{DC}, I_p, and ω_p encompass a parameter space of hundreds of thousands of reasonable and distinguishable configurations. Due to the nature of TWPAs, this parameter space also contains many local minima and maxima that prevent a gradient descent style of search (see section 5.2). Looking for the optimal operating configuration through brute-force effort would take weeks of experimental time in the cryogenic environment — this is not ideal for TWPA development, especially at the stage where such devices still potentially have many unexplored functionalities beyond amplification.

3.2 Automating data collection

Our automation software was designed and written in Python to efficiently set the parameter configurations of the signal generator and current source, and measure the resulting gain curves with the VNA. Built with extensibility in mind, the code is simplified through an abstraction layer (see figure 4) of generic signal generator, current source, and VNA objects used throughout the main automation logic. The user simply needs to select hardware-specific drivers that handle device-level

2024 JINST 19 P08024

communication over the VISA protocol, using PyVISA [26]. This modularity allows for quick development of the codebase, the extensibility required to accommodate future equipment, and the ability to make device-specific optimisations without re-writing the core logic.

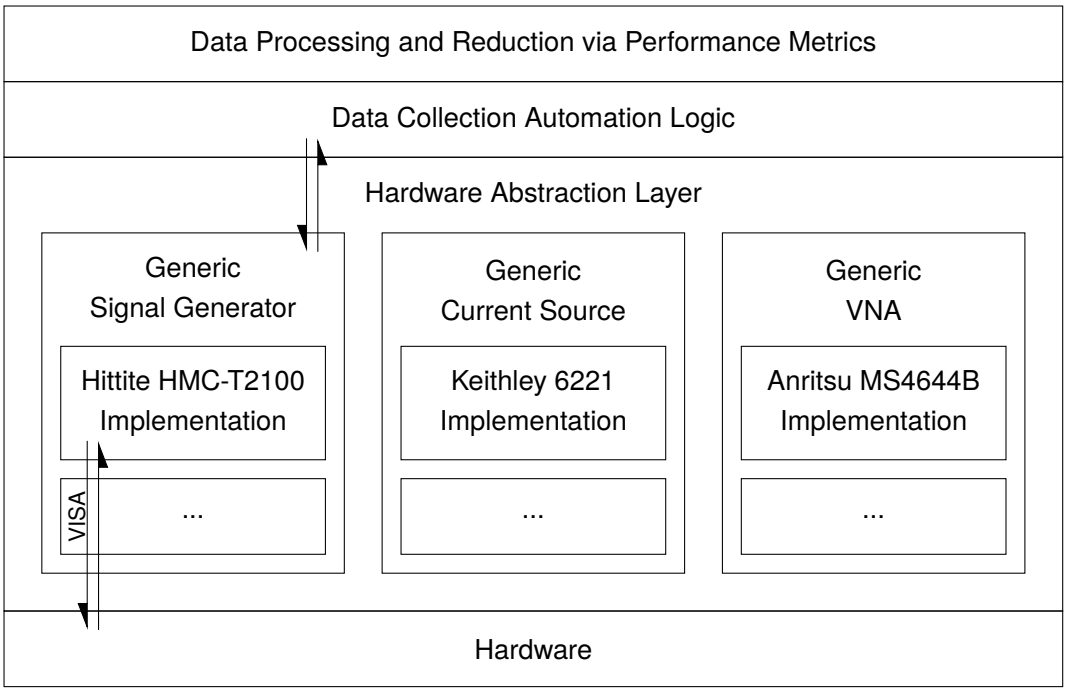

Figure 4. The automation software architecture showing the abstraction layers of generic equipment objects.

The main automation loop aims to mimic the manual method of varying device parameters, but with much more efficient speed. A user provides a range of pump frequencies, pump powers, and DC biases, and the software iterates through each possible configuration using three nested loops (see algorithm 1). Each non-bolded step within the algorithm requires interaction with the experimental apparatus, which takes several seconds for a human, but is almost instantaneous for the automation software. As a result, the code reduces the measurement time for setting a configuration and recording the result from tens of seconds when performed manually to less than 2 s, which is largely limited by the sweeping time of the VNA.

Careful consideration was made to ensure the DUT undergoes minimal time in the non-superconducting state, which occurs when the applied currents exceed the superconducting critical current, and cause the base temperature to rise rapidly. To avoid this, current and power values are always swept upwards from their minimum, and as soon as the software detects the device ceased being superconducting, all power is removed before starting the next iteration, after a short interval to ensure that the base temperature returns to its coldest state. If normal conduction occurs in the middle of the pump power loop, then the remaining pump powers for that pump frequency and DC bias are skipped, since they are higher than this empirically-determined critical power for the given DC bias, most probably due to defects in the device. If normal conduction occurs however at the beginning of the pump power loop (i.e. before any pump has been applied, so the DUT must have already passed the DC critical current threshold), then the remaining DC biases are skipped, and the algorithm moves to the subsequent pump frequency to be tested.

2024 JINST 19 P08024

Algorithm 1 Sweep a set of configurations and record the resulting gain curves.

Input: f_p, an array of pump frequencies
Input: I_p, an array of pump powers, sorted from smallest to largest
Input: I_DC, an array of DC biases, sorted from smallest to largest

```
for all f ∈ f_p do
    pump frequency ← f
    pump power ← 0 mW
    DC bias ← 0 mA
    for all i ∈ I_DC do
        DC bias ← i
        if not superconducting then
            DC bias ← 0 mA
            break
        else
            for all p ∈ I_p do
                pump power ← p
                if not superconducting then
                    pump power ← 0 mW
                    DC bias ← 0 mA
                    break
                else
                    SaveGainCurve(f, p, i)
                end if
            end for
        end if
    end for
end for
```

The detection of whether the device is in the superconducting or normal state is made through two redundant steps, ordered to optimise speed. First, the compliance state of the current source is queried to check if its compliance voltage was reached, which occurs when the resistance of the device increases from 0 Ω to ∼ MΩ upon going normal. A second contingency check is made by measuring the S_{21} data from the VNA. A portion of the normalised gain curve is averaged, and compared to a threshold value (−1.0 dB was chosen for the NbTiN TWPA). If the gain curve average falls below this value i.e., the device has become lossy over a wide frequency range, then superconductivity has likely been broken.

In practice, this second step is rarely required (except in the case where the DC bias is removed, with the current source set to 0 A), but can be relevant if a single small hot-spot within the TWPA breaks superconductivity without the entirety of the line going normal. As a result, non-superconducting states are detected extremely quickly, and the device temperature is maintained below 20 mK throughout continuous measurement. As a comparison, during manual variation of parameters, the temperature would regularly increase to ∼ 100 mK due to the slower human response of turning off the applied currents.

2024 JINST 19 P08024

3.3 Using the software for experiments

The methodology described above takes approximately 1.5 s to complete each loop (with the equipment detailed in section 2.2). Whilst this is much quicker than manual operation, it is still not feasible to sweep through a vast parameter space at an arbitrarily high resolution in a finite amount of time. As a result, a sweeping methodology is implemented:

1. Using knowledge from the design of the DUT and initial (limited) manual tests, sweep through a wide range of each parameter, in crude low-resolution steps. This will characterise the broad-scale behaviour of the device, and reveal a better and narrower parameter range to target. The number of configurations to be targeted could still range in the thousands, with a sweep taking from as little as an hour or two, to an overnight run for a more exhaustive broader-range search.

2. From the resulting areas of interest observed in step one, fix one of the three parameters, and vary the remaining two in high-resolution. For example,

   (a) Fix the pump frequency, and vary the pump power and DC bias in high resolution; or

   (b) Fix the pump power, and vary the pump frequency and DC bias in high resolution; or

   (c) Fix the DC bias, and vary the pump frequency and pump power in high resolution.

   This improves the characterisation of the fine-scale structure of the device. Multiple sweeps may be carried out, with the fixed parameter anchored at two or three different values. Although this may not account for interactions between all three parameters, it helps to show the potential influences of fine-structure effects.

3. Sweep within a restricted region of interest defined from step one, and step sizes set by the scale of features obtained from step two. The main aim of this step is to find the final configuration of the DUT that can achieve the optimal gain-bandwidth profile. As previously mentioned, a high-resolution sweep over a broad parameter range is extremely time-consuming and it can be difficult to maintain the cryogenic environment as stable as it is during these characterisation periods. A targeted sweep therefore accelerates the finding of the optimal configuration, without going through parameter space already identified in previous steps as sub-optimal (i.e., steps one and two). Even with all these pre-sifting exercises, it is noteworthy to stress that the number of configurations to be targeted for optimal gain could still range in the hundreds-of-thousands to millions per run, with a full sweep taking place over roughly two day's time.

The result of these automated measurements is a data cube (see figure 5), where each cell contains an individual frequency response for the given configuration of parameters labelled by the axes (pump frequency, pump power, and DC bias). Since the parameter space could be either two or three dimensional, with each of the hundreds of thousands of points corresponding to a gain curve, it is not feasible to sort through all the resulting data manually. Therefore, we further developed automated methods to summarise and visualise the device performance, to assist subsequent scientific evaluations.

2024 JINST 19 P08024

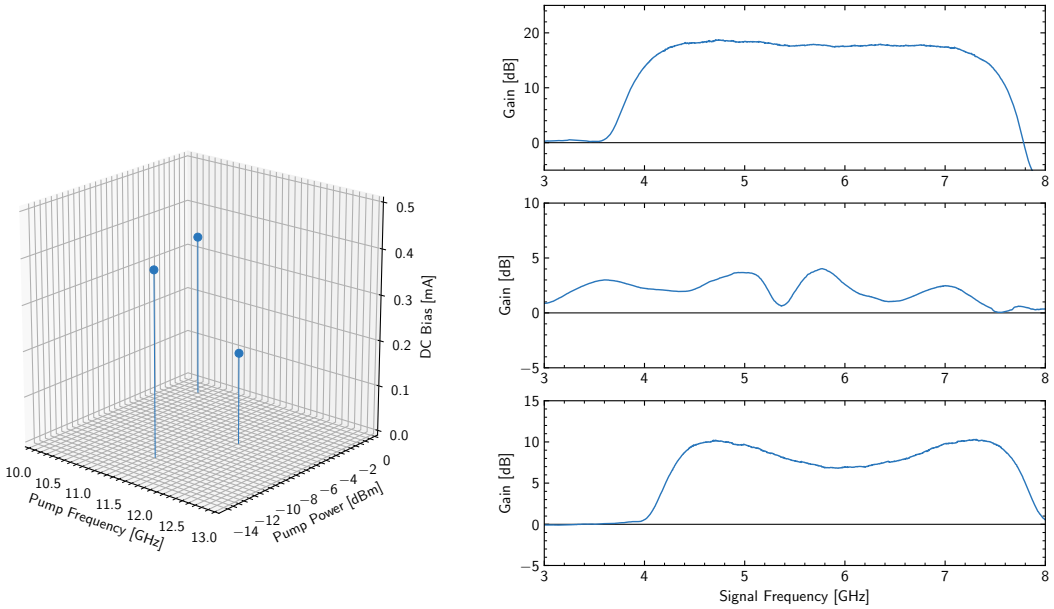

Figure 5. (Left) Illustration of the data cube obtained from an automated parameter sweep, with each cell representing an individual gain curve. We have only highlighted three cells to demonstrate this point. (Right) The three selected cells with their frequency responses for demonstration of the variation of gain profiles within the vast parameter space.

4 Data reduction and visualisation

Defining the condition for an optimal gain curve is not trivial; there are a number of metrics that could be used to measure success. Some applications may only require narrowband amplification, in which case the peak gain of a frequency-response curve is likely the most interesting parameter. Other applications may require broad-band amplification, hence the gain-bandwidth product (GBWP) is more likely to be more relevant. Furthermore, in many applications, the operational stability of the amplifier over a given frequency band is essential, meaning that the consistency of the frequency-response would be an important consideration. Whilst preliminary assessments of gain curves can be quickly made by the human eye, it is a less trivial operation in automation software, and care must be taken when defining the performance metric and interpreting its values.

Figure 6 shows an example gain curve that would be used to evaluate the performance metrics. In the following, we will make use of the average gain profile (shown in blue) for analysis, with the measured gain curves smoothed by a flat rolling-window of chosen bandwidth (e.g. 200 MHz for our DUT). This smoothing algorithm retains the original number of measured data points and their frequency-spacing without any artificial interpolation. As a result, the peak-gain metric is limited by the spacing of the VNA measurement points. Regions of the frequency responses can also be discounted (by setting their gain to say 0 dB) before performance metrics are evaluated. This step is taken due to the stop bands present in the TWPA responses (as a result of the dispersion-engineering described above). Within these regions, gain measurements obtained from the VNA are often artificially large, hence without discounting values within these stop bands, the performance metrics may risk being wildly skewed.

2024 JINST 19 P08024

After addressing all these pre-cautious steps, for narrowband high-gain applications, it is trivial to identify the average peak gain from the measured curve. However, for broadband applications, careful considerations are needed to define the maximum outcome required. Whilst the average peak gain shown in the blue curve of figure 6 is a reasonable 10 dB, the response shows a clear two-lobed behaviour, with the central region dropping to around only 7 dB. Should we define the maximum GBWP as the largest rectangular area that can be drawn under the gain curve e.g., the dash-dot region that reaches $\sim$ 7 dB over a roughly 3 GHz bandwidth, this could potentially underestimate the true GBWP in an actual application. Alternatively, we could instead evaluate performance by setting a user-defined threshold of minimal useable gain (say 8 dB), search for any regions that meet this criteria regardless of overall shape, and use an integral metric to calculate the area. This sums all the applicable regions to give a single metric for a given response: in the case of figure 6, the two lobes meet this criteria, and their integral-sum (the blue shaded regions) give an area of roughly 20 dB GHz.

We stress that these three evaluation methods of peak gain, maximum GBWP, and integral will result in different outcomes; hence choosing an appropriate performance metric is important to ensure the characterisation process can accurately sift the DUT's optimal performance for a particular application. We include all these options in our code (again developed using packages within the Python ecosystem [27–34]) and provide the flexibility within our module for incorporating new evaluation metrics for future applications.

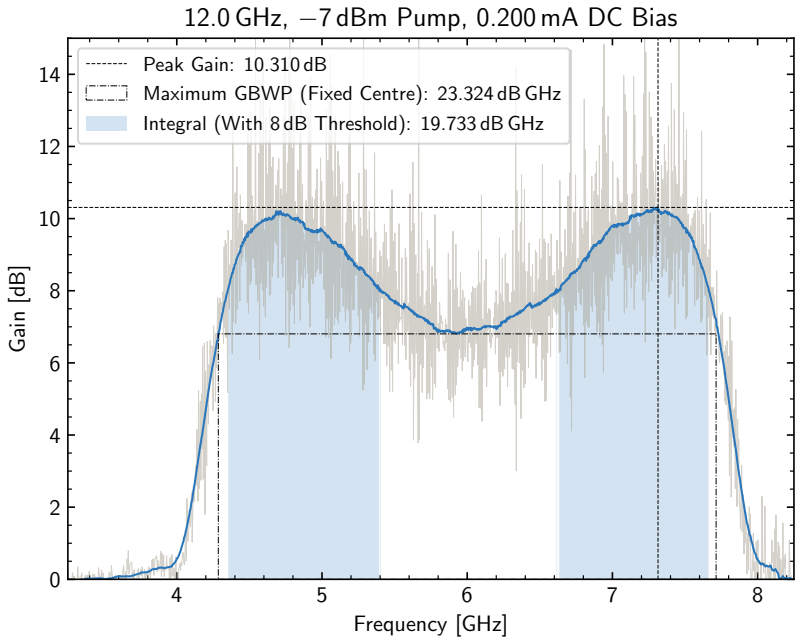

Figure 6. An example of a frequency response to show the difference in determining the three different performance metrics explained in the main text: the search for peak gain, the maximum GBWP rectangle, and an integration of regions meeting a user-defined gain threshold. The raw data is sampled with 4 MHz steps and shown in grey, and the average data from smoothing with a 200 MHz window is shown in blue. Note the listed pump power is before the attenuation shown in figure 2.

Whilst the performance metrics reduce the vast frequency response down to a single summary statistic, the configuration sweep across three tunable parameters still leaves us with a large cube

2024 JINST 19 P08024

of data to visualise. The simplest way to further visualise this and seek optimal configuration is to collapse the cube and project a 2D plot, by comparing two parameters of interest (e.g. pump power and DC bias) whilst varying the third parameter to maximise the plotted values.

5 Results

Here, we present a sample of automation results from characterising the NbTiN TWPA following the methods discussed above. The design of the device suggests a search with pump frequency around 11 GHz, pump powers[4] of ~ -5 dBm, and DC biases up to a critical current of roughly 0.5 mA. Using the methodology laid out in section 3.3, a number of characterisation sweeps were completed, searching for both broad- and fine-scale structure. The maximum GBWP performance metric was used for all plots in this section.

5.1 Broad-scale structure observations

The initial automated search was performed over a short sweep near the theoretically-designed optimal parameters. Figure 7 shows the maximum-value projections of each side of the resulting maximum GBWP data cube. The black regions with high DC bias and/or pump power are areas where superconductivity had already been broken, and the DUT returns to its normal state. Conversely, the black regions at lower DC bias and/or pump power are cases where the system simply has too little added energy to provide sufficient amplification of signals i.e., the gain curve is at the 0 dB level.

The patterns shown in figure 7 yield a number of insights. First, we see the general region of parameter space that provides good gain with pump frequencies ranging from 11 to 12 GHz, a DC bias supplied from 0.1 to 0.35 mA, and pump powers from -10 to 0 dBm. The relationship between the gain and the combination of pump power and DC bias can clearly be observed, with the diagonal shape of the lower-right plot showing how amplification is dependant on the combined power from the bias and pump, as expected. Furthermore, the sharp cutoff between superconducting and normal conduction states clearly shows the combined AC + DC critical current of the device, especially in the top-left and bottom-right plots. A region with better performance occurs near mid-range DC biases between 0.1 and 0.35 mA, combined with higher pump powers, around -12 to -2 dBm.

5.2 Fine-scale structure

Although the resulting plots in figure 7 are insightful, it is obvious that there is a substantial variation between adjacent pixels, especially in the regions of high gain. This indicates that the step sizes used in generating this data cube are insufficient to resolve the full detail of the performance of this device. To investigate the fine structure of the true TWPA performance with respect to operating parameters, we performed a number of high-resolution sweeps by fixing one parameter (either pump frequency, pump power, or DC bias) while allowing the other two to vary with a very fine step size. Note that full three-parameter sweeps are possible, but would require much longer measurement time.

Figure 8 shows the high-resolution sweeps obtained with the pump frequency fixed at 11.0 GHz, 11.5 GHz, and 12.0 GHz. Whilst the broad-scale combinatory dependence of the DC bias and pump power remains as expected, this fine-scale sweep yields much greater detail: we see clear periodic gain oscillations depending on the DC bias current that resemble a comb-like structure as the pump power

[4]Note all values for pump power are before the attenuation shown in figure 2.

2024 JINST 19 P08024

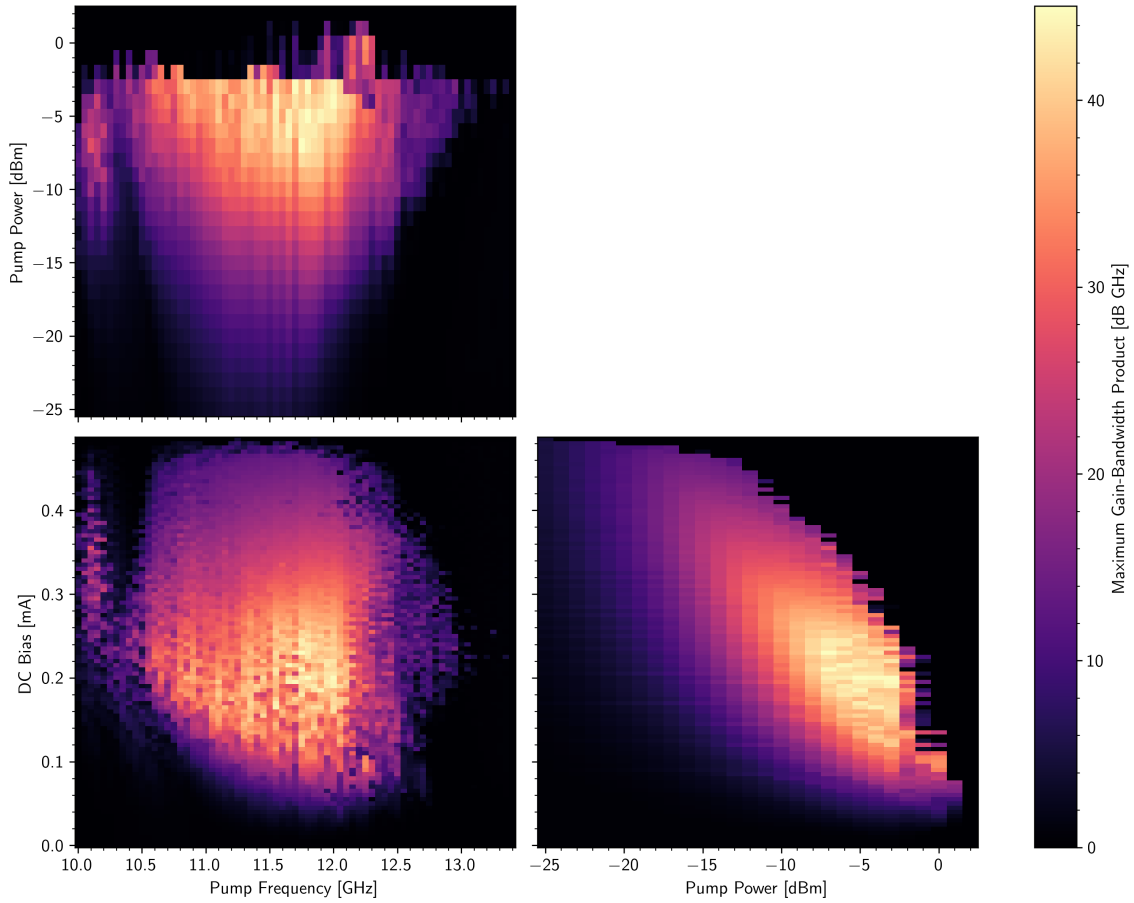

Figure 7. Maximum-value GBWP representation, collapsing the 3D cube obtained from a low-resolution sweep into 2D projections. This sweep targets the ranges 10 GHz $\leq f_p \leq$ 13.4 GHz in steps of 50 MHz, −25 dBm $\leq I_p \leq$ 4 dBm in steps of 1 dBm, and 0 mA $\leq I_{DC} \leq$ 0.5 mA in steps of 0.005 mA; a parameter-space of over 209,000 configurations.

increases, something not seen earlier in figure 7. A complete theoretical analysis and investigation into the root-cause of these results is still ongoing and beyond the scope of this work. The structure most likely arises from the effective shift in frequency response of the DUT, which constructively and destructively interferes with an applied current [35]. For example, in the case where the pump frequency is fixed at a position for maximal gain, when the DC bias current is varied, the kinetic inductance of the film is altered, thereby changing the internal reflections that impact the standing wave nature of the pump and therefore the amplitude of the gain. Furthermore, at high pump powers, parasitic resonances and other (unaccounted for theoretically) parametric processes become relevant that create instabilities in the gain or significantly alter its profile. This can be seen in the shift or breakdown of regularity close to the superconducting/normal conduction barrier, and is especially prominent when the pump frequency is detuned from 11.5 GHz and less well phase-matched.

This result highlights a significant issue not observed before: the importance of carefully choosing the parameter configuration required to properly operate the DUT. Naively, one may initially choose an operating point where the gain is highest and the bandwidth is the broadest, at a peak of the comb-like structure. Theoretically, this is ideal, but in practice, it may not be the best operating condition. As

2024 JINST 19 P08024

explained earlier, and visibly obvious from figure 8, a small change in the operational parameters could result in large changes in the characteristics of the DUT. This directly translates to the operational instability undesired in many applications. For example, small fluctuations in the signal generator or current source used could cause a large change in the DUT's performance — either the reduction of the gain profile, or in the case that the DUT returns to its normal state, a complete collapse of gain altogether. Additionally, as the TWPA is sensitive to the external environment, noisy equipment with rapidly-changing fluctuations could exacerbate this effect. Therefore, this heat-map is essential for allowing the user to carefully choose an optimal operating configuration, balancing the desired high GBWP and required stability for the DUT's chosen application.

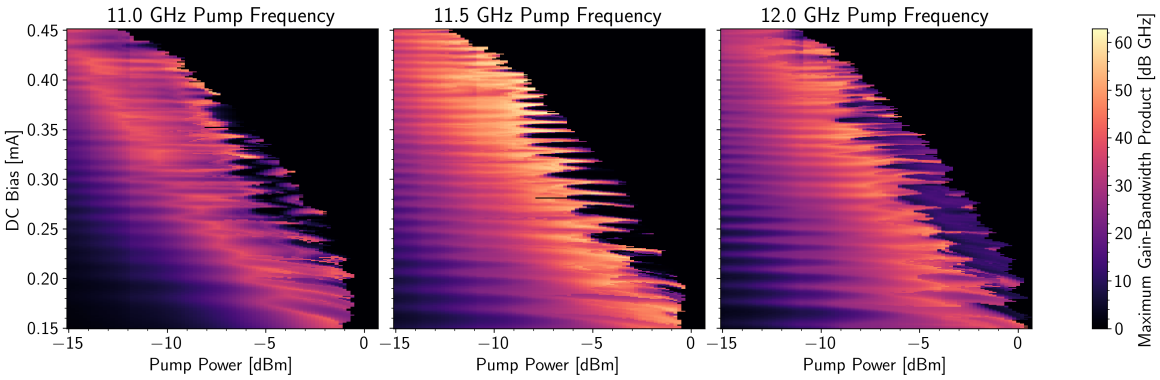

Figure 8. Maximum GBWP performance metric for the fine structure sweep, with pump frequency fixed at 11.0 GHz, 11.5 GHz, and 12 GHz, targeting the ranges $-15\,\text{dBm} \leq I_\text{p} \leq 4.8\,\text{dBm}$ in steps of 0.2 dBm, and $0.15\,\text{mA} \leq I_\text{DC} \leq 0.45\,\text{mA}$ in steps of 0.001 mA; this is a parameter-space of over 90,000 configurations.

To illustrate the effect, figures 9 and 10 compare two sets of configurations with identical parameters, except for an offset of 5 µA in the DC bias values. The pair in figure 9 are taken from close to the superconducting/normal conduction boundary, whereas the pair in figure 10 are at a lower pump power and higher DC bias. Whilst both regions can produce around 15 to 20 dB gain across a bandwidth of $\sim$ 3 GHz, the one closest to the superconducting/normal conduction boundary is clearly much less stable.

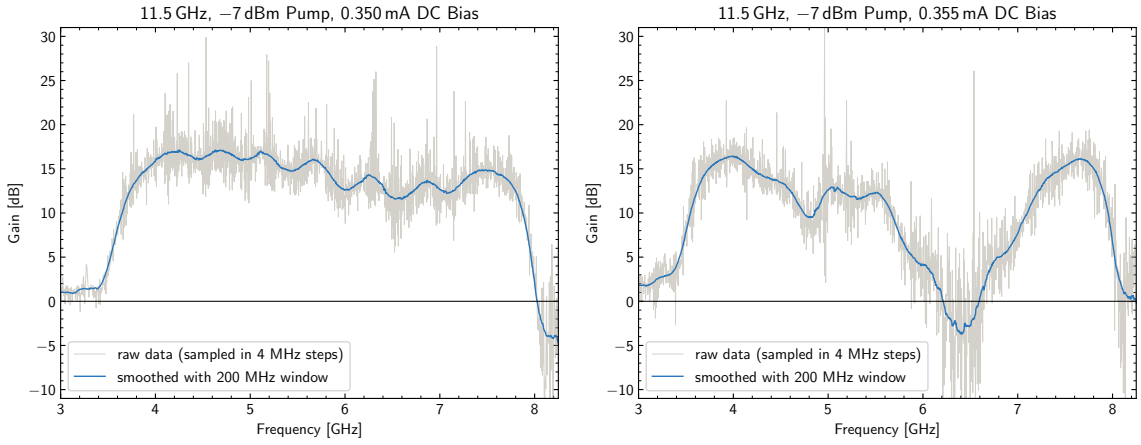

Figure 9. A pair of identical configurations (except for an offset of 5 µA in the DC bias) taken from near the superconducting/normal conduction boundary.

2024 JINST 19 P08024

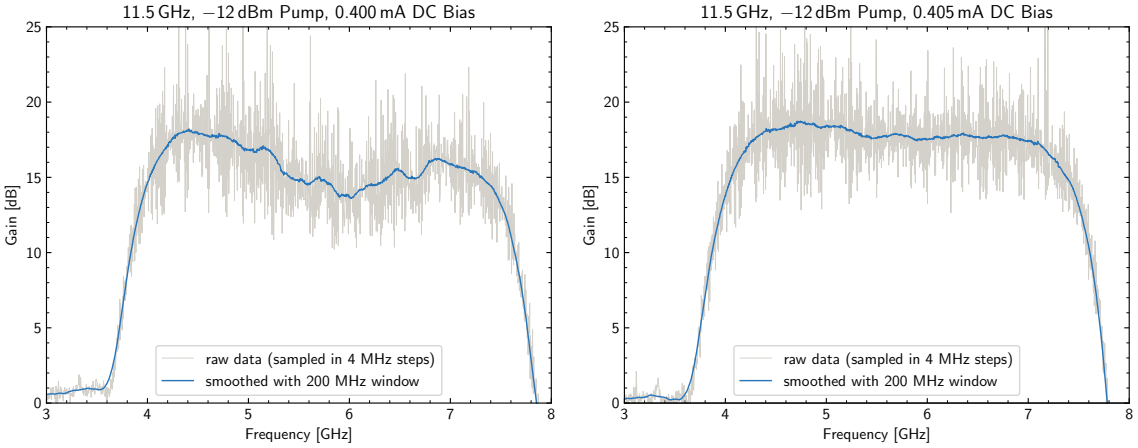

Figure 10. A pair of identical configurations (except for an offset of 5 µA in the DC bias) taken away from the superconducting/normal conduction boundary.

Figure 11 shows the result of another high-resolution sweep with the pump power fixed at −5 dBm instead. As expected, the device performs better with increasing DC bias. Periodic oscillations in gain with respect to pump frequency are expected as changes in the pump frequency shift the standing wave structures intrinsic to the TWPA. However, unexpectedly, figure 11 shows that this variation becomes less rapid with increasing DC bias current.

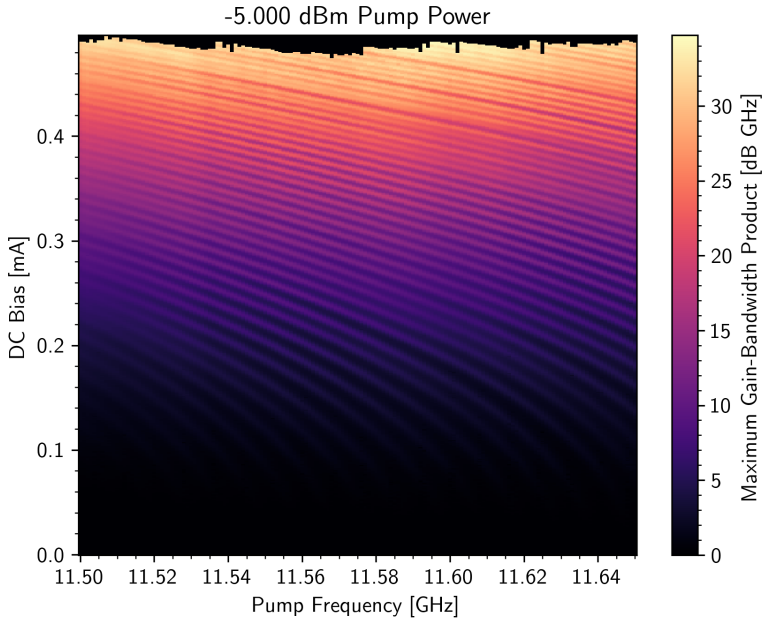

Figure 11. Maximum GBWP performance metric values for the fine sweep with fixed pump power. The sweep targeted the ranges 11.50 GHz $\leq f_p \leq$ 11.65 GHz in steps of 1 MHz, and 0 mA $\leq I_{DC} \leq$ 0.5 mA in steps of 1 µA; this parameter-space results in over 75,000 configurations.

This pump-frequency variation can be seen more clearly in figure 12, which displays a high-resolution sweep fixing the DC bias at 0.350 mA. The sharp contrast of the vertical lines shows that

2024 JINST 19 P08024

there is a significant variation in the resulting maximum GBWP as the pump frequency is adjusted on the order of MHz. Furthermore, the upper cutoff power at which the critical current is reached varies wildly with pump frequency, likely also due to the standing wave reflections in the device, which have a similar periodicity of ~ 8 MHz, which reduces by ~ 1 % at the maximal bias current. Note also that the maximum GBWP for both figure 8 and figure 12 are higher than that in figure 7, indicating that a very fine search of the parameter space is required to obtain maximum gain in a TWPA.

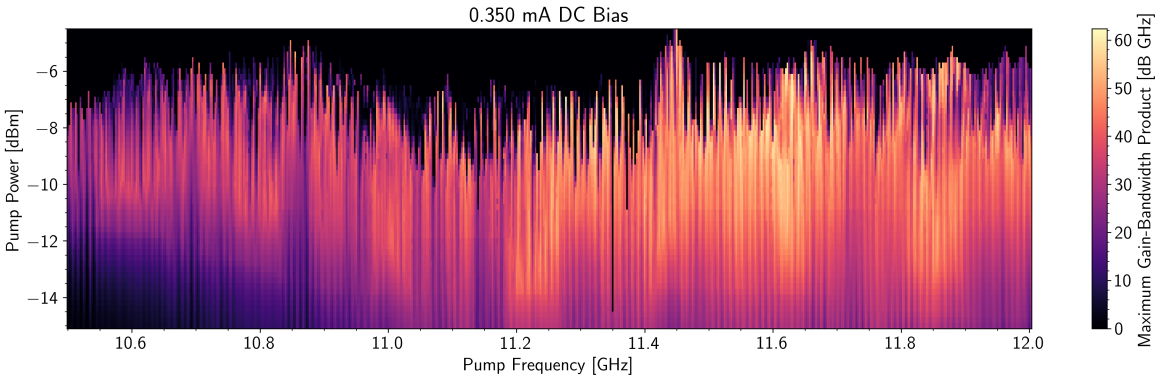

Figure 12. Maximum GBWP performance metric values for a fine-structure sweep, fixing the DC bias current. The sweep targeted the ranges 10.5 GHz $\leq f_p \leq$ 12.0 GHz in steps of 2.5 MHz, and -15.0 dBm $\leq I_p \leq$ 4.8 dBm in steps of 0.2 dBm; this is a parameter-space of over 60,000 configurations.

It is noteworthy that the swiftly-oscillating comb-like characteristics of the DUT are not anticipated through fundamental theoretical analysis and design of the TWPA. These features would likely be overlooked in manual DUT characterisation, underscoring the significance of our automation software in fully unveiling the authentic behaviour of the DUT. This, in turn, guides the user in determining the optimal and most stable configuration of the TWPA during practical operation.

6 Discussion

As demonstrated earlier, our methodology reveals insights that surpass what can be discerned through manual characterisation within a practical timeframe. It is essential to reiterate that this methodology can yield measurements equivalent to nearly one person-month of continuous, non-stop measurement in just a single night. This rapid automation enabling exploration across extensive parameter spaces inevitably results in a substantial amount of data. As an indication, each VNA scan produces an S2P (two-port scattering-parameters matrix) file with a size on the order of approximately 1 MB. For some of the results presented earlier, we generated close to 1 TB of data within two to three days of automated measurement. Nonetheless, the analysis component of the software efficiently allows us to compress, sift through, and process this massive volume of data in less than an hour, and discard redundant data cubes. It further enables the generation of concise plots summarising device performance, to unveil previously unknown behaviour of the DUT and offer meaningful interpretations for further analysis.

The primary advantage of SPAs and TWPAs lies in their quantum noise-limited performance, a feature leveraged to enhance the resolution of MKIDs [36] and achieve improved sensitivity in dark matter searches [37]. Notably, in certain experiments, a broad bandwidth is not always imperative. Some experiments focus on a narrower range of frequencies dictated by other experimental constraints, such as

2024 JINST 19 P08024

the resonant cavity in a dark matter search experiment [38]. In these cases, the key performance metric for SPAs/TWPAs becomes the maximum achievable gain at a specific frequency and time, aligning with the tuning of the remaining experimental setup — specifically e.g., the tuning frequency of the cavity. This imposes a distinct requirement on the SPA/TWPA performance: rather than necessitating high gain across a wide range of frequencies simultaneously, it calls for an exceptionally high gain across a narrower frequency range that can be subsequently tuned to sweep through the larger frequency range.

As depicted in figures 9 and 10, the unsmoothed gain profile of the DUT exhibits a rippling feature that varies significantly with signal frequency and is highly sensitive to the applied pump and DC parameters. In the context of the applications described earlier, attention is redirected to metrics like figure 13, which illustrates the maximum achievable gain measured for a given signal frequency. While achieving this response requires multiple parameter sets (a different one for each signal frequency), it highlights the tunability of the TWPA to deliver substantial narrowband gain over a broad signal frequency range, by sweeping through it using the operating parameters table obtained from our automated fine-structure sweeps. The profile in figure 13, condensed from hundreds of thousands of gain curves, underscores the significance of the automation and analysis presented in this work. Without these tools, utilising a TWPA to attain such elevated levels of narrowband gain would be practically impossible.

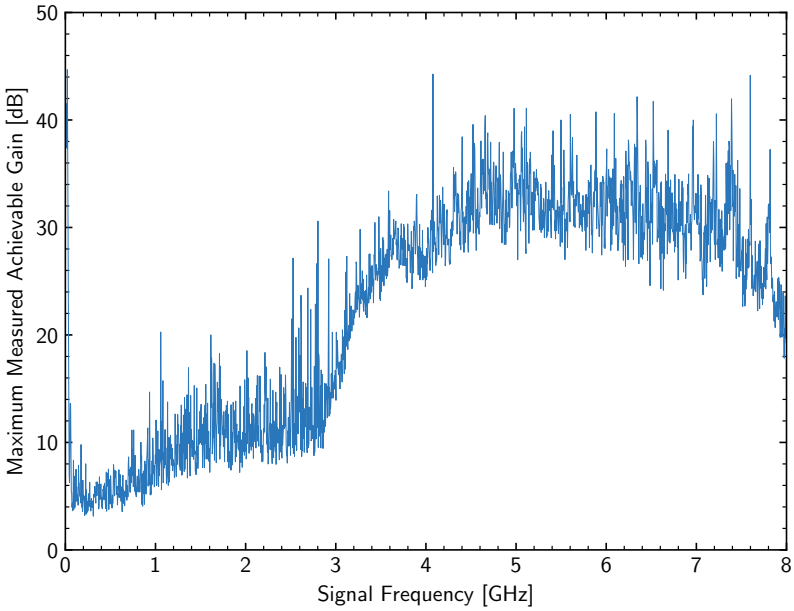

Figure 13. The NbTiN TWPA's maximum measured achievable gain at a given signal frequency (1 kHz bandwidth sampled every 4 MHz). Collated from the frequency responses previously summarised in section 5. The peak at 10 MHz is an artifact resulting from the high-pass cutoff of the amplifiers, bias tees, and directional coupler in the setup causing all measurements at that point to be near the VNA noise floor.

7 Conclusion

While parametric amplifiers, such as SPAs and TWPAs, boast numerous strengths that render them advantageous across a wide range of applications, the need for meticulous fine-tuning of their operating parameters beyond the design stage introduces a substantial volume of manual work. The

2024 JINST 19 P08024

computer automation methodology we have demonstrated facilitates a detailed characterisation of how a parametric amplifier responds to different configurations of parameters in real-life experimental conditions. Using our existing NbTiN TWPA device, we showcased that our methodology unveils unexpected fine structure behaviour, a task nearly impossible with manual characterisation techniques alone. This revelation not only discloses new insights but also prompts a reconsideration of the operational aspects of an SPA or TWPA, emphasising not only high gain over a broad bandwidth but also the stability of such operation. We also introduce a novel operational mode for a TWPA, specifically an extremely high gain amplifier with multiple operating parameters at each signal frequency. This achievement is made possible through our fine-structure scan of a TWPA. The efficiency of this automation setup extends beyond identifying suitable operating conditions for various SPAs in different scenarios; it provides profound insights into how a device responds to different parameters. This capability holds great promise for future investigations in the field of parametric amplification research and development, as the software architecture was designed to be applicable to all types of SPAs, including JPAs, kinetic inductance, Josephson junctions, and SQUIDs (Superconducting Quantum Interference Devices) TWPAs. Moreover, it allows for potential expansion to encompass other superconducting quantum devices.

Acknowledgments

This research was funded by the European Research Council (ERC) under the European Union's Horizon 2020 research and innovation programme with grant agreement No. [803862] (Project [SPA4AstroQIT]). For the purpose of Open Access, the author has applied a CC BY public copyright license to any Author Accepted Manuscript version arising from this submission.

References

[1] B. Ho Eom, P.K. Day, H.G. LeDuc and J. Zmuidzinas, *A wideband, low-noise superconducting amplifier with high dynamic range*, *Nature Phys.* **8** (2012) 623.

[2] M. Malnou et al., *Performance of a Kinetic Inductance Traveling-Wave Parametric Amplifier at 4 Kelvin: Toward an Alternative to Semiconductor Amplifiers*, *Phys. Rev. Appl.* **17** (2022) 044009.

[3] C. Bockstiegel et al., *Development of a Broadband NbTiN Traveling Wave Parametric Amplifier for MKID Readout*, *J. Low Temp. Phys.* **176** (2014) 476.

[4] K. Peng et al., *Floquet-Mode Traveling-Wave Parametric Amplifiers*, *PRX Quantum* **3** (2022) 020306.

[5] J.Y. Qiu et al., *Broadband squeezed microwaves and amplification with a Josephson travelling-wave parametric amplifier*, *Nature Phys.* **19** (2023) 706 [arXiv:2201.11261].

[6] K. O'Brien, C. Macklin, I. Siddiqi and X. Zhang, *Resonant Phase Matching of Josephson Junction Traveling Wave Parametric Amplifiers*, *Phys. Rev. Lett.* **113** (2014) 157001.

[7] B.-K. Tan et al., *Engineering the thin film characteristics for optimal performance of superconducting kinetic inductance amplifiers using a rigorous modelling technique*, *Open Res. Europe* **2** (2022) 88.

[8] W. Shan, Y. Sekimoto and T. Noguchi, *Parametric Amplification in a Superconducting Microstrip Transmission Line*, *IEEE Trans. Appl. Superconduct.* **26** (2016) 1.

[9] S. Zhao, S. Withington, D.J. Goldie and C.N. Thomas, *Loss and saturation in superconducting travelling-wave parametric amplifiers*, *J. Phys. D* **52** (2019) 415301.

2024 JINST 19 P08024

[10] B.-K. Tan et al., *Operation of kinetic-inductance travelling wave parametric amplifiers at millimetre wavelengths*, *Superconduct. Sci. Technol.* **37** (2024) 035006.

[11] S. Chaudhuri, J. Gao and K. Irwin, *Simulation and Analysis of Superconducting Traveling-Wave Parametric Amplifiers*, *IEEE Trans. Appl. Superconduct.* **25** (2014) 1.

[12] S. Zhao and S. Withington, *Quantum analysis of second-order effects in superconducting travelling-wave parametric amplifiers*, *J. Phys. D* **54** (2021) 365303.

[13] N. Klimovich, S. Wood, P.K. Day and B.-K. Tan, *Investigating the effects of sum-frequency conversions and surface impedance uniformity in traveling wave superconducting parametric amplifiers*, *J. Appl. Phys.* **135** (2024) 124402.

[14] M. Malnou et al., *Three-Wave Mixing Kinetic Inductance Traveling-Wave Amplifier with Near-Quantum-Limited Noise Performance*, *PRX Quantum* **2** (2021) 010302.

[15] S. Goldstein et al., *Four wave-mixing in a microstrip kinetic inductance travelling wave parametric amplifier*, *Appl. Phys. Lett.* **116** (2020) 152602.

[16] S. Chaudhuri et al., *Broadband parametric amplifiers based on nonlinear kinetic inductance artificial transmission lines*, *Appl. Phys. Lett.* **110** (2017) 152601.

[17] C. Macklin et al., *A near–quantum-limited Josephson traveling-wave parametric amplifier*, *Science* **350** (2015) 307.

[18] H.R. Nilsson et al., *High-Gain Traveling-Wave Parametric Amplifier Based on Three-Wave Mixing*, *Phys. Rev. Appl.* **19** (2023) 044056 [arXiv:2205.07758].

[19] L. Planat et al., *Photonic-Crystal Josephson Traveling-Wave Parametric Amplifier*, *Phys. Rev. X* **10** (2020) 021021.

[20] A.B. Zorin, *Josephson Traveling-Wave Parametric Amplifier with Three-Wave Mixing*, *Phys. Rev. Appl.* **6** (2016) 034006.

[21] D. Cunnane et al., *High-efficiency Ka-band frequency multiplier based on the nonlinear kinetic inductance in a superconducting microstrip*, *Appl. Phys. Lett.* **124** (2024) 022601.

[22] G. Butseraen et al., *A gate-tunable graphene Josephson parametric amplifier*, *Nature Nanotech.* **17** (2022) 1153 [arXiv:2204.02175].

[23] J.C. Longden and B.-K. Tan, *Non-degenerate-pump four-wave mixing kinetic inductance travelling-wave parametric amplifiers*, *Eng. Res. Express* **6** (2024) 015068.

[24] N. Klimovich et al., *Demonstration of a Quantum Noise Limited Traveling-Wave Parametric Amplifier*, arXiv:2306.11028.

[25] N. Klimovich, *Traveling Wave Parametric Amplifiers and Other Nonlinear Kinetic Inductance Devices*, Ph.D. thesis, Caltech, Pasadena, U.S.A. (2022).

[26] H.E. Grecco et al., *PyVISA: the Python instrumentation package*, *J. Open Source Softw.* **8** (2023) 5304.

[27] C.R. Harris et al., *Array programming with NumPy*, *Nature* **585** (2020) 357 [arXiv:2006.10256].

[28] P. Virtanen et al., *SciPy 1.0–Fundamental Algorithms for Scientific Computing in Python*, *Nature Meth.* **17** (2020) 261 [arXiv:1907.10121].

[29] J.D. Hunter, *Matplotlib: A 2D Graphics Environment*, *Comput. Sci. Eng.* **9** (2007) 90.

[30] A. Arsenovic et al., *scikit-rf: An Open Source Python Package for Microwave Network Creation, Analysis, and Calibration [Speaker's Corner]*, *IEEE Microwave* **23** (2022) 98.

[31] K. Goodman and Bottleneck Developers, *Bottleneck*, https://github.com/pydata/bottleneck.

2024 JINST 19 P08024

[32] M. Siemens, *TinyDB*, https://github.com/msiemens/tinydb/.

[33] M.M. McKerns et al., *Building a Framework for Predictive Science*, in the proceedings of the *10th Python in Science Conference*, Austin, TX, 11-116 July 2011 [arXiv:1202.1056].

[34] M.M. McKerns and M.A.G. Aivazis, *pathos: a framework for heterogeneous computing*, https://uqfoundation.github.io/project/pathos.

[35] R. Basu Thakur et al., *Superconducting On-chip Fourier Transform Spectrometer*, *J. Low Temp. Phys.* **200** (2020) 342 [arXiv:1909.02100].

[36] N. Zobrist et al., *Wide-band Parametric Amplifier Readout and Resolution of Optical Microwave Kinetic Inductance Detectors*, *Appl. Phys. Lett.* **115** (2019) 042601 [arXiv:1907.03078].

[37] K. Ramanathan et al., *Wideband Direct Detection Constraints on Hidden Photon Dark Matter with the QUALIPHIDE Experiment*, *Phys. Rev. Lett.* **130** (2023) 231001 [arXiv:2209.03419].

[38] N. Tomita et al., *Search for hidden-photon cold dark matter using a K-band cryogenic receiver*, *JCAP* **09** (2020) 012 [arXiv:2006.02828].

2024 JINST 19 P08024